FARADAY

Kinetics of the HO_2 + BrO reaction over the temperature range 233–348 K

Zhuangjie Li,† Randall R. Friedl and Stanley P. Sander*
M/S 183-901, Jet Propulsion Laboratory, California Institute of Technology, Pasadena, California 91109, USA

The reaction BrO + HO_2 → products is the rate-limiting step in a key catalytic ozone destruction cycle in the lower stratosphere. In this study a discharge-flow reactor coupled with molecular beam mass spectrometry has been used to study the BrO + HO_2 reaction over the temperature range 233–348 K. Rate constants were measured under pseudo-first-order conditions in separate experiments with first HO_2 and then BrO in excess in an effort to identify possible complications in the reaction conditions. At 298 K, the rate constant was determined to be $(1.73 \pm 0.61) \times 10^{-11}$ cm^3 molecule^{-1} s^{-1} with HO_2 in excess and $(2.05 \pm 0.64) \times 10^{-11}$ cm^3 molecule^{-1} s^{-1} with BrO in excess. The combined results of the temperature-dependent experiments gave the following fit to the Arrhenius expression: $k = (3.13 \pm 0.33) \times 10^{-12} \exp(536 \pm 206/T)$ where the quoted uncertainties represent two standard deviations. The reaction mechanism is discussed in light of recent *ab initio* results on the thermochemistry of isomers of possible reaction intermediates.

Introduction

Bromine chemistry plays a key role in the catalytic destruction of stratospheric ozone. The most important bromine-containing source gas, methyl bromide, has an ozone depletion potential which exceeds the limits set by international treaties, and will be phased out in developed countries by the year 2010.[1] However, because methyl bromide has both biogenic and anthropogenic source fluxes which are highly uncertain, the budgets and atmospheric lifetime of methyl bromide have not been accurately determined. Most other bromine source gases of importance, including the halons, are entirely anthropogenic in origin and their production has ceased in developed countries. Despite the regulatory controls in place, however, there are many issues relating to both the gas-phase and heterogeneous chemistry of bromine compounds that require further investigation.

The catalytic cycles that contribute to the destruction of ozone by bromine were first described by Wofsy *et al.*[2] and Yung *et al.*[3] By analogy to the well known O + ClO cycle, Wofsy *et al.* proposed the cycle

$$\begin{aligned} &\mathrm{Br} + \mathrm{O_3} \rightarrow \mathrm{BrO} + \mathrm{O_2} && (1)\\ &\mathrm{BrO} + \mathrm{O} \rightarrow \mathrm{Br} + \mathrm{O_2} && (2)\\ \text{Net}\quad &\mathrm{O} + \mathrm{O_3} \rightarrow 2\mathrm{O_2} \end{aligned}$$

This cycle has its greatest effect on ozone destruction in the middle and upper stratosphere. Yung *et al.* pointed out several additional cycles that are particularly important in the lower stratosphere that couple bromine radicals with the odd hydrogen and odd chlorine radical families:

$$\begin{aligned} &\mathrm{Br} + \mathrm{O_3} \rightarrow \mathrm{BrO} + \mathrm{O_2}\\ &\mathrm{BrO} + \mathrm{HO_2} \rightarrow \mathrm{HOBr} + \mathrm{O_2} && (3)\\ &\mathrm{HOBr} + h\nu \rightarrow \mathrm{OH} + \mathrm{Br}\\ &\mathrm{OH} + \mathrm{O_3} \rightarrow \mathrm{HO_2} + \mathrm{O_2}\\ \text{Net}\quad &2\mathrm{O_3} \rightarrow 3\mathrm{O_2} \end{aligned}$$

and

$$\begin{aligned} &\mathrm{Br} + \mathrm{O_3} \rightarrow \mathrm{BrO} + \mathrm{O_2}\\ &\mathrm{Cl} + \mathrm{O_3} \rightarrow \mathrm{ClO} + \mathrm{O_2}\\ &\mathrm{BrO} + \mathrm{ClO} \rightarrow \mathrm{Br} + \mathrm{Cl} + \mathrm{O_2} && (4)\\ \text{Net}\quad &2\mathrm{O_3} \rightarrow 3\mathrm{O_2} \end{aligned}$$

In these cycles, reactions (3) and (4) are the rate-limiting steps. Reaction (4) has been studied extensively over the temperature and pressure range relevant to the stratosphere and is reasonably well understood.[4,5] In contrast, significant kinetic and mechanistic uncertainties remain in the understanding of reaction (3).

The first study of reaction (3) was carried out by Cox and Sheppard who reported a rate coefficient of $0.5^{+0.5}_{-0.3} \times 10^{-11}$ cm^3 molecule^{-1} s^{-1} at 303 K and 760 Torr total pressure using molecular-modulation coupled with UV absorption.[6] Three recent studies, however, have reported values of k_{298} which were more than six times larger than the work of Cox and Sheppard including two discharge-flow/mass spectrometry studies from the CNRS group and a flash photolysis/ultraviolet absorption study from the group at Bordeaux.[7–9] These measurements have a major effect on atmospheric model predictions of bromine partitioning in the lower stratosphere, the relative magnitudes of the odd oxygen destruction cycles involving bromine and the ozone depletion potential of methyl bromide.[1,7] More recently however, a discharge-flow/mass spectrometry study by Elrod *et al.*[10] reported a significantly smaller value of k_{298}, $(1.4 \pm 0.3) \times 10^{-11}$ cm^3 molecule^{-1} s^{-1}.

The large discrepancies between the previously reported results and the importance of this reaction in stratospheric bromine chemistry motivated the study reported here. In this work, the BrO + HO_2 reaction was investigated over the temperature range 233–348 K using the discharge-flow/mass spectrometry technique. In an effort to identify possible complications in the reaction conditions, rate coefficients were measured using several different BrO and HO_2 sources and separately with BrO and HO_2 as the excess reagent.

† Present address: Department of Atmospheric Sciences, University of Illinois, Urbana, IL 61801-3070, USA.

Experimental

The experimental apparatus used in these studies has been described previously.[11,12] Details of the flow reactor and sliding injector are shown in Fig. 1. The reactor consisted of an 80 cm long, 4.86 cm id Pyrex tube which was covered on the inside with a layer of 0.05 cm thick TFE Teflon sheet to reduce BrO and HO_2 wall loss. The reactor temperature was varied between 233 and 348 K by circulating cooled methanol or heated ethylene glycol through an outer Pyrex jacket. The temperatures of the circulating fluids were measured with a thermocouple located in the outer jacket of the reactor and controlled to within ± 2 K using a thermostatted heat exchanger. A steady-state gas flow (total pressure of 1–3 Torr) was maintained in the flow tube with a 100 cubic feet per minute mechanical pump (Welch 1396). Helium was used as the main buffer gas and was admitted through a side-arm located upstream of the reactor. The mean gas velocity in the flow tube ranged between 800 and 2000 cm s^{-1}; resulting in residence times between 30 and 75 ms in the 60 cm reaction zone. In order to carry out kinetics measurements at low temperatures, a heated double sliding injector was employed. It consisted of two concentric tubes having internal diameters of 8 and 10.2 mm, respectively. The movable injector was heated by passing current through heating wire wrapped around the outer injector tube. This tube was thermally isolated from the flow tube with a vacuum jacket. The injector temperature was controlled by varying the voltage applied to the heating wire and measured with a thermocouple contacting the outer surface of the injector. Measurements showed that for a reactor wall temperature of 233 K, a constant temperature of 298 K could be maintained inside the injector. Under these conditions the temperature of the outer surface of the injector vacuum jacket was 280 K. As discussed below, we found that heating the injector was very important in minimizing complications associated with the production of BrO and HO_2 at low temperatures.

Mass spectrometric detection of reactants and products was carried out by continuous sampling at the downstream end of the flow tube through a three-stage differentially pumped beam inlet system. The mass spectrometer (Extrel Model C50) consisted of an electron-impact ionizer, a quadrupole mass filter, and a channeltron detector. Beam modulation was accomplished with a 200 Hz tuning fork type chopper placed inside the second stage of the mass spectrometer. Ion signals from the channeltron were sent to a lock-in amplifier that was referenced to the chopper frequency. The amplified analogue signals were digitized (Analog Devices RTI/815) and recorded by a microcomputer.

Radical production

In order to minimize systematic errors caused by unknown secondary reactions in the radical sources, the main flow tube and the reactor walls, we used several different reactions to produce BrO and HO_2 and the kinetic runs were carried out with both BrO and HO_2 as the excess reagent. The radical source conditions are summarized in Table 1 and described in detail below.

Two methods were used to produce BrO: (*a*) reaction of Br_2 with atomic oxygen generated by microwave discharge of O_2–He,

$$O + Br_2 \rightarrow BrO + Br \quad (5)$$

$$k_5(298\ K) = 1.4 \times 10^{-11}\ cm^3\ molecule^{-1}\ s^{-1}\ (ref.\ 13)$$

and (*b*) reaction of ozone with bromine atoms generated in a microwave discharge of Br_2–He,

$$Br + O_3 \rightarrow BrO + O_2 \quad (1)$$

$$k_1(298\ K) = 1.2 \times 10^{-12}\ cm^3\ molecule^{-1}\ s^{-1}\ (ref.\ 4)$$

For either of these source reactions, BrO radicals undergo rapid self-reaction, producing Br with about 85% efficiency at

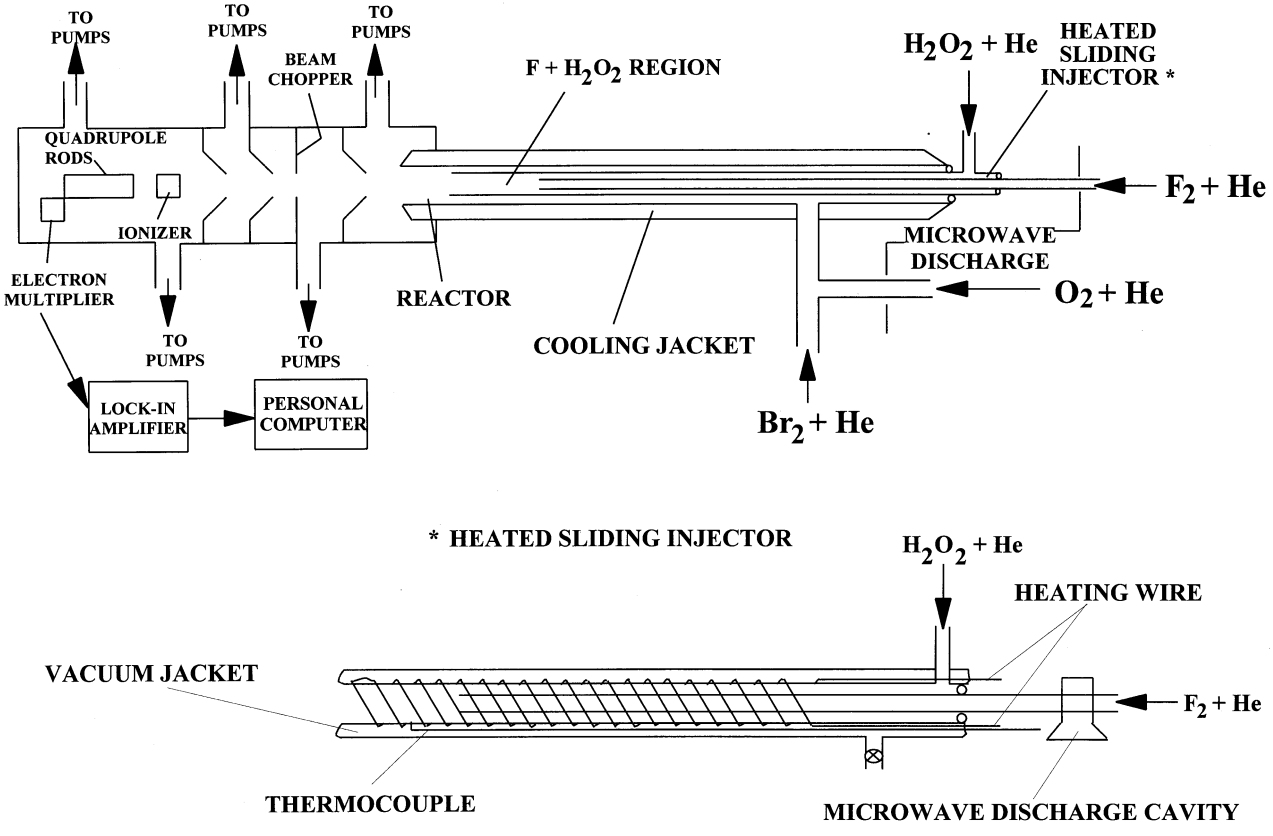

Fig. 1 Schematic diagram of the experimental apparatus for the study of BrO + HO_2 kinetics

Table 1 Summary of radical source reactions and reactor conditions for the BrO + HO_2 reaction

radical	reagent stoichiometry	source reaction(s)	source location	flow-tube temperature/°C	concentration /10^{12} molecule cm^{-3}
HO_2	excess	F + H_2O_2	injector	253–298	1–8
HO_2	minor	Cl + CH_3OH	side-arm	233–348	0.1–1.5
BrO	excess	Br + O_3	injector	233–348	1–5
BrO	minor	O + Br_2	side-arm	253–298	0.1–0.5

room temperature:

$$BrO + BrO \rightarrow 2Br + O_2 \quad (6)$$

$$k_6(298\ K) = 2.1 \times 10^{-12}\ cm^3\ molecule^{-1}\ s^{-1}\ (ref.\ 4)$$

The highest concentrations of BrO were obtained using the Br + O_3 source in the presence of an excess of O_3. In this case, Br formed in reaction (6) was rapidly recycled back to BrO. For the Br + O_3 source, *ca.* 4×10^{13} molecule cm^{-3} of Br_2 was flowed through a 1.27 cm od quartz discharge tube with 350 standard cubic centimetres per minute (sccm) helium carrier gas. After passing through the 30 cm long central injector tube, *ca.* $(1–10) \times 10^{14}$ molecule cm^{-3} of O_3 was introduced through the side-arm of the injector with 50 sccm of helium carrier gas, producing $(1–5) \times 10^{12}$ molecule cm^{-3} BrO radicals in the reactor. The O + Br_2 source was unable to produce BrO at these concentrations due to the lower microwave discharge efficiency of oxygen and BrO recombination, but this source was satisfactory for use in experiments where HO_2 was the excess reagent.

For the generation of HO_2, two separate methods were used: (*a*) reaction of hydrogen peroxide with atomic fluorine generated from microwave discharge of F_2,

$$F + H_2O_2 \rightarrow HO_2 + HF \quad (7)$$

$$k_7(298\ K) = 4.98 \times 10^{-11}\ cm^3\ molecule^{-1}\ s^{-1}\ (ref.\ 14)$$

and (*b*) reaction of atomic chlorine from microwave discharge of Cl_2 with methanol followed by further reaction with oxygen,

$$Cl + CH_3OH \rightarrow CH_2OH + HCl \quad (8)$$

$$k_8(298\ K) = 5.4 \times 10^{-11}\ cm^3\ molecule^{-1}\ s^{-1}\ (ref.\ 4)$$

$$CH_2OH + O_2 \rightarrow HO_2 + CH_2O \quad (9)$$

$$k_9(298\ K) = 9.1 \times 10^{-12}\ cm^3\ molecule^{-1}\ s^{-1}\ (ref.\ 4)$$

As in our previous studies of HO_2 kinetics using this apparatus,[15] we found that method (*a*) was suitable for producing large concentrations of HO_2 at room temperature. Using the same side-arm arrangement as used for Br + O_3 with the quartz discharge tube replaced by an alumina tube, a small flow (5–20 sccm) from a premixed 5% F_2–He cylinder was mixed with a larger (400 sccm) helium flow which passed through the discharge. Dissociation of F_2 was typically >90%. Water was added through the side-arm of the movable injector with 650 sccm of helium carrier gas bubbling through the 90% H_2O_2 solution. The reaction of F with H_2O_2 was complete within 1 ms and the initial F atom concentration, and thus the HO_2 concentration, was adjusted by varying the F_2 flow. About 10^{14} molecule cm^{-3} of H_2O_2 was brought into the injector, and the production of HO_2 in the reactor was initially in the range $(1–8) \times 10^{12}$ molecule cm^{-3}. This method was restricted to temperatures above 253 K due to condensation of H_2O_2 and H_2O on the flow tube walls which resulted in very high wall loss rates for HO_2.

Using method (*b*), chlorine atoms were formed by discharging a flow of 5–10 sccm of 1% Cl_2 in helium to which was added an additional helium flow of 250–500 sccm. Chlorine atoms reacted in the side-arm with CH_3OH obtained from a 5–10 sccm helium flow through a methanol saturator held at a pressure of 400 Torr and a temperature of 25 °C. An oxygen flow of 20–40 sccm was added along with the methanol. Using this method the highest HO_2 concentration that could be produced was *ca.* 1.5×10^{12} molecule cm^{-3}. The major difficulty with this method was that flowing a large quantity of methanol into the reactor created a large $m/z = 33$ background signal which interfered with the HO_2 radical detection. This interference decreased substantially with decreasing methanol concentration. Thus for kinetics studies of reaction (3) with BrO in excess, method (*b*) was used to produce HO_2 as the minor reagent.

Both BrO and HO_2 radicals were detected using electron impact ionization mass spectroscopy at the parent peaks, $m/z = 95$ (BrO^+) and $m/z = 33$ (HO_2^+). When H_2O_2 was used as the HO_2 precursor, there was an $m/z = 33$ contribution arising from the fragmentation of H_2O_2 and from the wing of the much larger m/z 34 peak. This interference was minimized by optimizing the quadrupole resolution and the ionizer electron energy. Table 2 shows the $m/z = 33$ signal intensity as function of electron energy for the F + H_2O_2 system. It can be seen that the ratio of HO_2 signal to background $m/z = 33$ contribution was maximized at an electron energy of 19 eV, which was subsequently used in all kinetics studies.

Absolute concentrations of both BrO and HO_2 were calibrated by chemical conversion to NO_2 with an excess of NO, *i.e.*

$$BrO + NO \rightarrow Br + NO_2 \quad (10)$$

$$HO_2 + NO \rightarrow OH + NO_2 \quad (11)$$

This was accomplished by introducing the BrO or HO_2 radicals from the movable injector and NO from the side-arm of the reactor, with the injector placed in a downstream position such that the reaction time between NO and the calibrated radical was ⩽3 ms. The concentration of added NO was in the range $(1–5) \times 10^{14}$ molecule cm^{-3}. The conversion factors were determined from the ratio of the change in NO_2 ion signal at m/z 46, S_{46}, to the change in the radical signal, S_{95} or S_{33}. ($\Delta S_{46}/\Delta S_{95} = 0.40 \pm 0.08$ and $\Delta S_{46}/\Delta S_{33} = 1.8 \pm 0.4$).

Table 2 Signal (mV) at $m/z = 33$ as a function of ionizer electron energy for the F + H_2O_2 system[a]

	ionizer electron energy/eV								
signal source	25	24	23	22	21	20	19	18	17
(*a*) signal from F + H_2O_2	643	510	473	365	300	220	155	85	35
(*b*) signal from H_2O_2 alone	230	170	115	79	48	29	15	8.6	4.0
[(*a*) − (*b*)]/(*b*)	1.8	2.0	3.1	3.6	5.3	6.6	9.3	8.9	7.8

[a] Emission current = 1.0 mA.

The radical calibrations were then obtained from absolute calibrations of the mass spectrometer at m/z 46 using known concentrations of NO_2.

Special care was taken for the HO_2 calibration since HO_2 could be regenerated by the reactions,

$$OH + H_2O_2 \rightarrow H_2O + HO_2 \quad (11)$$

$k_{11}(298\ K) = 1.7 \times 10^{-12}$ cm^3 molecule^{-1} s^{-1} (ref. 4)

or

$$OH + CH_3OH \rightarrow H_2O + CH_2OH$$

$$CH_2OH + O_2 \rightarrow CH_2O + HO_2$$

One way to prevent this HO_2 regeneration in the titration was adding a large excess (*ca.* 10^{15} molecule cm^{-3}) of C_2F_3Cl which reacts rapidly with OH to form a stable adduct.[16,17] However, it was found that this concentration of C_2F_3Cl reduced the responsivity of the mass spectrometer by *ca.* 6% owing to a reduction in the efficiency of the ionizer. An alternative OH scavenger which had a negligible effect on the mass spectrometer was molecular bromine, Br_2. The reaction of Br_2 with OH is very fast,

$$Br_2 + OH \rightarrow HOBr + Br \quad (12)$$

$k_{12}(298\ K) = 4.2 \times 10^{-11}$ cm^3 molecule^{-1} s^{-1} (ref. 4)

thus when 5×10^{13} molecule cm^{-3} of Br_2 was introduced into the reactor, the OH radical was scavenged in less than 0.5 ms. The product of the OH + Br_2 reaction, HOBr, had no effect on the calibration. The detection limits for the radicals were 2×10^9 molecule cm^{-3} for BrO and 8×10^9 molecule cm^{-3} for HO_2 (S/N = 2 for a 10 s integration time).

First-order wall loss coefficients were measured for both HO_2 and BrO and found to be <5 s^{-1} at low radical concentrations ($<5 \times 10^{11}$ molecule cm^{-3}). For the runs with excess HO_2, the effective wall loss increased at the highest HO_2 concentrations, presumably due to the HO_2 self-reaction. As a first-order approximation, the HO_2 concentration for the kinetic run was derived by averaging the concentrations at the upstream and downstream ends of the reaction zone. Simulations showed that the error arising from this approximation was $\leqslant 5\%$. In the case of excess BrO, the same procedure was employed although the wall loss was always <4 s^{-1}.

The gases used in this work had the following stated purities: He, 99.999%; NO, 99%; NO_2, 99.5%; Cl_2 (10% in He); F_2 (5% in He) and O_2 (99.999%). Br_2 (99.8%) was purified by vacuum distillation at 195 K. H_2O_2 was obtained commercially at a concentration of 70 wt.% and purified to $\geqslant 94$ wt.% prior to use by vacuum distillation at room temperature. Ozone was produced by passing O_2 through an ozonizer and storing the product on silica gel at 195 K. During the experiments, O_3 was maintained at 195 K and evaporated into the reactor with a known flow of He. In order to avoid the potential explosion hazard associated with the condensation of ozone in the liquid-nitrogen trap of the mechanical pump, efforts were made to decompose the ozone downstream of the flow tube. This was accomplished efficiently by heating the effluent from the flow tube to *ca.* 300 °C in a 50 cm long quartz tube containing copper scouring pads.

Pressure measurements were made using capacitance manometers that were calibrated against NBS standards. Gas flow measurements were made with electronic flowmeters calibrated using the bubble displacement method. The estimated systematic uncertainties of the experimental measurements at the 95% confidence level are: pressure (±1%), gas flow rates (±3%), detector non-linearity (±2%), absolute calibration of the mass spectrometer responsivity (±20%). These systematic errors were combined in quadrature with the observed random errors to give the experimental uncertainties in the derived rate constants.

Results

Measurements of k_3 were carried out by monitoring the decay of either BrO or HO_2 as a function of reaction time. Bimolecular rate constants were obtained using the well-known steady-state flow-tube method,[12] in which the first-order decay rate constant, k'_3, was determined from the slope of a plot of the logarithm of either BrO or HO_2 signal *vs.* reaction time. In all experiments the minor reactant was introduced into the flow tube through a fixed side-arm and the excess reagent was added through the sliding injector. In experiments in which HO_2 was the minor species, the signal was corrected by subtracting the $m/z = 33$ signal contribution from the HO_2 precursors as discussed above. In these experiments, the H_2O_2 concentration did not change appreciably with injector position as determined from measurements of the m/z 34 peak. The observed decays were then corrected for axial diffusion and for loss of BrO or HO_2 on the injector according to eqn. (I),[12]

$$k'_{3,corr} = k'_3\left(1 + \frac{k'_3 D}{v^2}\right) + k_p \quad (I)$$

where D is the diffusion coefficient, v is the mean bulk flow velocity, and k_p is the first-order loss of BrO or HO_2 on the outside surface of the sliding injector (injector loss). Diffusion coefficient estimates were based on the data of Marrero and Mason.[18] The estimated D values for BrO varied from 0.43 atm cm^2 s^{-1} at 233 K to 0.84 atm cm^2 s^{-1} at 348 K and for HO_2 varied from 0.49 to 0.97 atm cm^2 s^{-1} over the same temperature range. The corrections for axial diffusion were always $<1\%$.

Kinetics of BrO and HO_2 decay at 298 K

A typical BrO decay as function of the injector position at 298 K is shown in Fig. 2. The BrO decay appeared to be exponential within the time domain studied, and the BrO was completely titrated to our detection limit at high HO_2 concentrations ($[HO_2] \geqslant 5 \times 10^{12}$ molecule cm^{-3}). With initial BrO concentrations of (2–5) $\times 10^{11}$ molecule cm^{-3} and HO_2 concentrations of (1–8) $\times 10^{12}$ molecule cm^{-3}, the dependence of k'_3 on $[HO_2]$ is shown in Fig. 3; k'_3 varied from 20 to 160 s^{-1} in the HO_2 concentration range of interest. Fig. 3 also shows the results of measurements of k'_3 taken over a range of flow velocities and total pressures to check for the presence of systematic errors such as bimolecular wall reactions. For flow velocities of 750–1800 cm s^{-1} and total reactor pressures of 1–3 Torr the first-order decay of BrO due to reaction with HO_2 was independent of these parameters. From

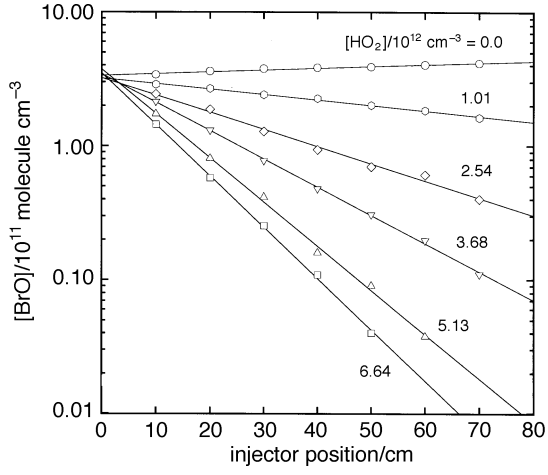

Fig. 2 BrO decay in the presence of excess HO_2 at 298 K. HO_2 was produced using the F + H_2O_2 source. HO_2 concentrations are in units of 10^{12} molecule cm^{-3}.

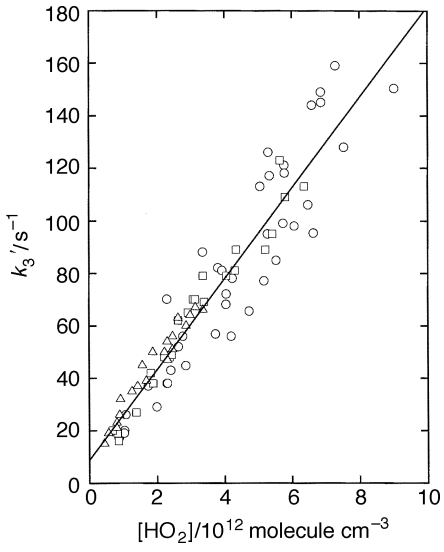

Fig. 3 First-order decay rate of BrO, k_3', as a function of $[HO_2]$ at 298 K. (□) $P_{total} = 1$ Torr and $v = 750$ cm s^{-1}, (○) $P_{total} = 1$ Torr and $v = 1600$ cm s^{-1}, (△) $P_{total} = 3$ Torr and $v = 1800$ cm s^{-1}, (——) best fit.

the slope of linear least-squares fit through all the data at 298 K, k_3 was determined to be $(1.73 \pm 0.61) \times 10^{-11}$ cm^3 $molecule^{-1}$ s^{-1}, where (and hereafter) the quoted uncertainty is at the 95% confidence level and includes both random and systematic errors.

The behavior of HO_2 in the presence of excess BrO was also investigated. Fig. 4 shows a typical HO_2 decay as function of injector position over the BrO concentration range $(1.3–4.5) \times 10^{12}$ molecule cm^{-3} at 298 K. Twenty four runs were performed at 298 K and the bimolecular rate coefficient for reaction (3) in excess BrO was derived as $(2.05 \pm 0.64) \times 10^{-11}$ cm^3 $molecule^{-1}$ s^{-1} from a linear least-squares fit to the data in Fig. 5.

Temperature dependence of the rate coefficient for reaction (3)

Rate constants for reaction (3) were measured over the temperature range 233–348 K using both excess BrO and excess HO_2 with the source reactions and inlet conditions shown in Table 1. Both secondary reactions and wall reactions limited the temperature range of the study. These complications will be discussed in detail below.

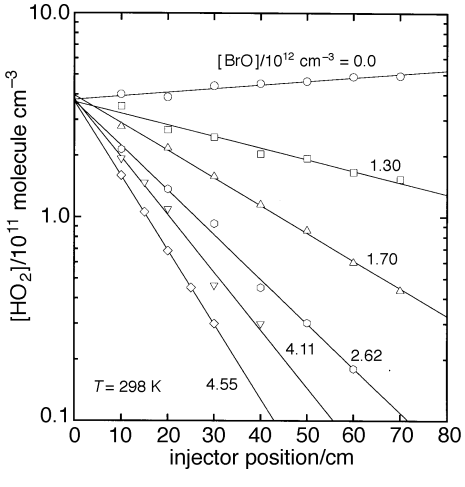

Fig. 4 HO_2 decay in the presence of excess BrO at 298 K. BrO was produced using the Br + O_3 source. BrO concentrations are in units of 10^{12} molecule cm^{-3}.

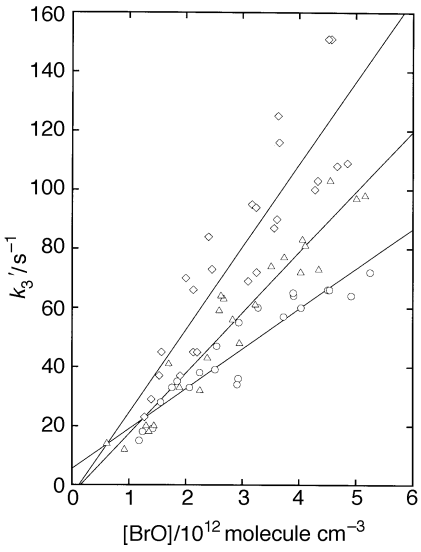

Fig. 5 First-order decay rates, k_3', of HO_2 as a function of [BrO] at 298 K (△), 253 K (◇) and 348 K (○)

At temperatures between 298 and 348 K, both the BrO (excess reagent, Br + O_3 source) and HO_2 (minor reagent, Cl + CH_3OH source) ion signals were well behaved with no significant complications. Above 348 K, there was significant regeneration of HO_2 as indicated by the $m/z = 33$ ion signal reaching a steady state at long reaction times ($t > 65$ ms). A possible explanation for this behavior is secondary production of HO_2 initiated by the thermal decomposition of HOBr:

$$HO_2 + BrO \rightarrow HOBr + O_2$$

$$HOBr + M \rightarrow OH + Br + M$$

$$OH + BrO \rightarrow HO_2 + Br$$

This effect limited to 348 K the maximum temperature for which reliable kinetics results could be obtained.

At temperatures below 298 K, a number of processes interfered with the production of both BrO and HO_2. For HO_2 produced using the F + H_2O_2 source, the maximum concentration that could be achieved decreased significantly below about 270 K. The dependence of the observed $m/z = 33$ signal on temperature is shown in Fig. 6. For these experiments, HO_2 was produced in an unheated injector and the temperature was measured in the flow-tube jacket which was not

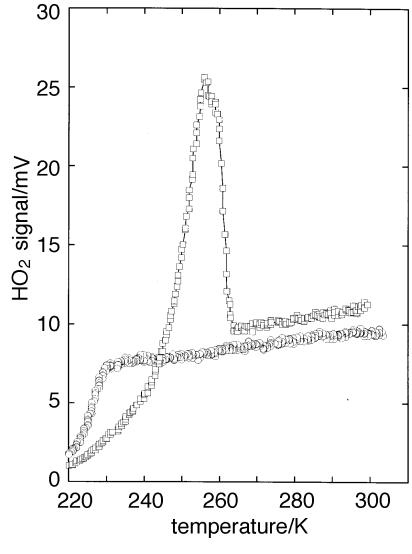

Fig. 6 HO_2 signal intensity as a function of flow-tube temperature using the F + H_2O_2 source; (○) cooling, (□) warming

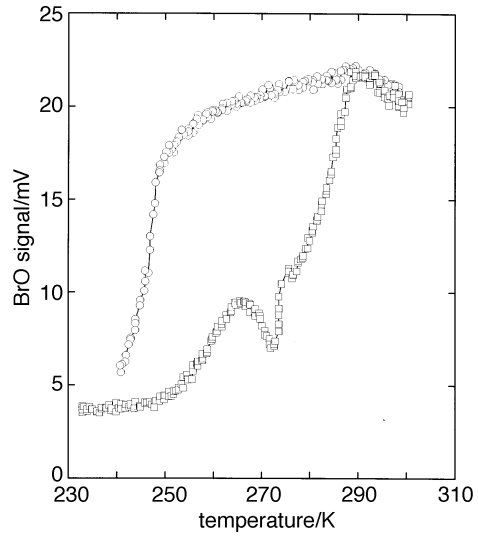

Fig. 7 BrO signal intensity as a function of flow-tube temperature using the O + Br_2 source; (○) cooling, (□) warming

in thermal equilibrium with the injector due to the time lag in cooling and heating. The observed signal decrease in the cooling cycle and increase in the heating cycle are attributed to adsorption and desorption of H_2O and H_2O_2 on the flow-tube and injector walls. The decrease in the HO_2 concentration is due to both an increase in the HO_2 wall loss rate on the coated surfaces and the removal of H_2O_2 from the gas phase. The use of the heated injector eliminated these problems in the injector itself, but deposition of H_2O and H_2O_2 on

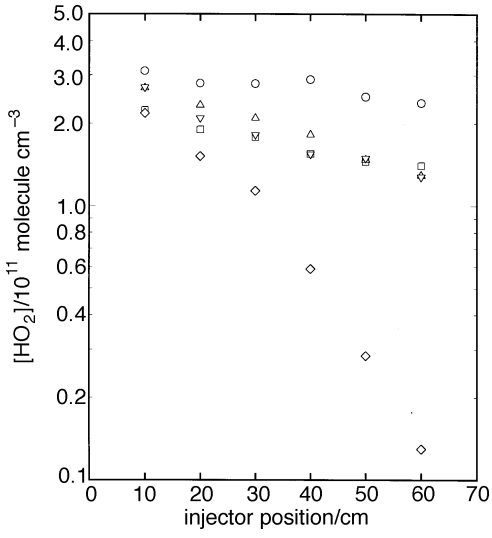

Fig. 8 Temporal decay of HO_2 in the absence of ClO as a function of reactor temperature (○) 298, (□) 273, (△) 253, (▽) 233, (◇) 213 K. The slopes of the lines are the effective wall loss rate constants for HO_2.

the flow-tube walls remained a problem at temperatures below 253 K. As in the experiments of Larichev *et al.*, we observed that the Cl + CH_3OH + O_2 source efficiency decreased rapidly at temperatures below about 250 K in the unheated injector. Larichev *et al.*[8] dealt with this problem by moving their HO_2 source reactor to a side-arm in the uncooled region of the flow tube, but since HO_2 was the excess reagent in their experiments, this introduced the first-order BrO wall loss into their observed decay rates. In our experiments at low temperatures, HO_2 was the minor reagent and the Cl + CH_3OH + O_2 source could be used in the side-arm at room temperature without requiring a separate measurement of the wall loss.

The temperature dependence of the BrO^+ ion signal using the O + Br_2 source in the side-arm is shown in Fig. 7. As in the case of HO_2, the BrO concentration in the flow tube displays a hysteresis in the cooling/warming cycle indicating the presence of complex wall reactions. Observation of the flow-tube surface at low temperature revealed a solid layer on the injector surface with a white–yellow color. This layer was observed using both the O + Br_2 and Br + O_3 sources. We further studied this solid layer using the heated injector. This was carried out by cooling the injector for 1 h with the BrO source on, then switching off the source and warming the injector while scanning the mass spectrometer for desorption products. Three major species were simultaneously detected at m/z = 95/97 (BrO^+), m/z = 111/113, ($OBrO^+$ or $BrOO^+$), and m/z = 174 (Br_2O^+), which peaked at injector temperatures of *ca.* 260, 270 and 280 K, respectively. Parent mass peaks corresponding to other higher oxides such as Br_2O_2, Br_2O_4 or Br_2O_7 could not be detected due to the mass range limit of the mass spectrometer, but if these species were formed, they would likely have fragmented and contributed to the daughter fragments indicated above.

Higher bromine oxides have been observed several times previously in discharge-flow/mass spectroscopy studies of oxygen–bromine systems.[8,19] The detailed formation mechanisms are not known but wall reactions play a key role in the formation and interconversion of the bromine oxides, and the primary products may be both OBrO and Br_2O.[20] The surface reactions appear to require the presence of $O(^3P)$ and/or metastable oxygen $O_2(^1\Delta, {}^1\Sigma)$ from the microwave discharge. In order to characterize the products of the wall reactions occurring in the flow reactor, separate experiments were carried out using similar discharge-flow systems coupled to UV–VIS and submillimeter absorption spectrometers.[21] In both systems, the product of an O_2 discharge reacted with a flow of Br_2 at low temperature (−20 °C) to form the same yellow–white solid observed in the DF/MS apparatus. The vapor from the solid was recorded by the spectrometers after the deposition of the solid was discontinued. In the UV–VIS apparatus, an intense progression of vibrational bands was observed in the 380–620 nm spectral region which was nearly identical to the spectrum observed by Rattigan *et al.* in the steady-state photolysis of Br_2–O_3 mixtures and assigned to OBrO.[22] In the submillimeter spectrometer, a large number of rotational lines were observed.[23] Analysis of the spectra iden-

Table 3 Summary of experimental conditions and measured rate constants for the reaction HO_2 + BrO → products

pressure/Torr	temperature/K	$k_3/10^{11}$ cm^3 molecule^{-1} s^{-1}	excess reagent
1	348	1.35 ± 0.44	BrO
1	323	1.76 ± 0.52	BrO
1	298	2.05 ± 0.64	BrO
1–3	298	1.73 ± 0.61	HO_2
1	273	2.62 ± 0.87	BrO
1	273	2.06 ± 0.62	HO_2
1	253	2.80 ± 1.11	BrO
1	253	2.32 ± 0.65	HO_2
1	233	3.06 ± 1.15	BrO

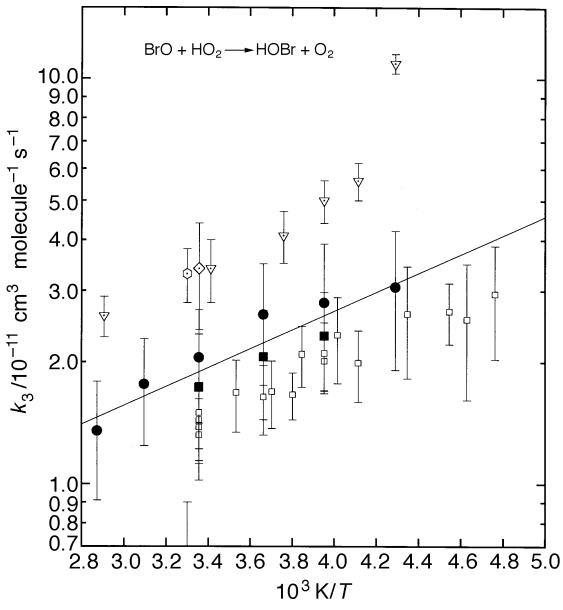

Fig. 9 Temperature dependence of the rate constant for the BrO + HO_2 reaction: (●) this work, excess HO_2; (■) this work, excess BrO; (⏀) Poulet *et al.*,[7] (▽) Larichev *et al.*;[8] (◇) Bridier *et al.*;[9] (□) Elrod *et al.*;[10] (——) best fit to data from this work

tified the source of the lines as isotopomers of both OBrO and Br_2O.

Adding NO to the desorbing species resulted in the formation of NO_2, most likely from the NO + OBrO reaction:

$$OBrO + NO \rightarrow BrO + NO_2$$

Under conditions where the bromine oxides were formed (low temperature, O + Br_2 source, unheated injector) this reaction interfered with the mass spectrometric calibration of BrO.

When the resistively heated injector was used, most of the problems associated with the low-temperature production of BrO and HO_2 were eliminated, and this system was used for all of the low-temperature studies. The wall loss of radicals at low temperatures was examined with the heated injector. The first-order BrO wall loss was negligible down to 210 K but the HO_2 wall loss increased significantly with decreasing temperature. As shown in Fig. 8, the HO_2 wall loss was *ca.* 7 s^{-1} at 298 K, increasing to 64 s^{-1} at 213 K. The large wall loss rate of HO_2 at low temperature restricted the range of reliable kinetics measurement for reaction (3) to 233 K and above.

Kinetics data were obtained over the temperature ranges 233–348 K with BrO in excess and 253–298 K with HO_2 in excess. The rate constant data are summarized in Table 3 and an Arrhenius plot as shown in Fig. 9. From these data it is apparent that the rate coefficient has a negative temperature dependence. For the three temperatures at which both excess BrO and excess HO_2 data are available, the rate constants using excess BrO are systematically 20–25% larger, but the data overlap within the $\pm 2\sigma$ error limits. Although the data show a small non-linear Arrhenius temperature dependence, the curvature lies well within the uncertainty of the measurements. A linear least-squares fit gives the following Arrhenius expression:

$$k_3 = (3.13 \pm 0.33) \times 10^{-12} \exp(536 \pm 206/T)$$

The reaction products for BrO + HO_2 were briefly studied with HO_2 in excess. HOBr was found to be the predominant reaction product based on approximate absolute mass spectrometric calibrations of HOBr. Small HBr mass peaks were also detected at 298 K, but it was not possible to ascribe them to the HBr formation channel of reaction (3) since other processes such as Br + HO_2 and Br + H_2O_2 and wall reactions could also contribute to HBr formation.

Discussion

Effects of secondary reactions

The agreement (within 20%) between rate coefficients obtained under excess HO_2 and excess BrO conditions shows that, in general, there are no significant complications from secondary reactions. There are, however, a few processes that need to be considered explicitly. The reaction

$$OH + BrO \rightarrow HO_2 + Br$$

$$k_{298} = 7.5 \times 10^{-11} \text{ cm}^3 \text{ molecule}^{-1} \text{ s}^{-1}$$

has been studied recently by Bogan *et al.*[24] and found to be significantly faster than previously estimated.[4] In the kinetic runs which used excess HO_2, simulations show that an OH impurity equal to about $0.2[HO_2]_0$ could effectively double the observed first-order disappearance rate of BrO under conditions where there are no other removal paths for OH. In our system, OH is formed in the HO_2 source as a result of the reaction of fluorine atoms with water vapor which is present as an unavoidable impurity in H_2O_2. Conditions in the source are adjusted in the H_2O_2 source to allow the fast reaction

$$OH + HO_2 \rightarrow H_2O + O_2$$

$$k_{298} = 1.1 \times 10^{-10} \text{ cm}^3 \text{ molecule}^{-1} \text{ s}^{-1}$$

to scavenge most of the OH on the timescale of the source chemistry. The HO_2 source should therefore be a negligible source of OH ($<1 \times 10^{10}$ molecule cm^{-3} in the flow tube). In addition, Br_2 is present at concentrations around 10^{13} molecule cm^{-3} from the BrO source. This concentration of Br_2 is sufficient to scavenge OH rapidly from the reaction

$$OH + Br_2 \rightarrow HOBr + Br$$

as discussed above. The absence of significant impurity concentrations of OH from the HO_2 source was verified in separate experiments which set a conservative upper limit of 10^{10} molecule cm^{-3} for HOBr when the HO_2 source was on and the BrO discharge was off.

The reaction

$$Br + HO_2 \rightarrow HBr + O_2$$

$$k_{298} = 2.0 \times 10^{-12} \text{ cm}^3 \text{ molecule}^{-1} \text{ s}^{-1}$$

is a potential secondary removal pathway for HO_2 in the excess BrO experiments because the BrO + BrO reaction is a

Table 4 Comparison of rate constant measurements for the reaction HO_2 + BrO → products

ref.	technique[a]	pressure/Torr	temperature/K	$k_3/10^{11}$ cm^3 molecule^{-1} s^{-1}
Cox and Sheppard[6]	MP/UV	760	303	$0.5^{+0.5}_{-0.3}$
Poulet *et al.*[7]	DF/MS	1	298	3.3 ± 0.5
Bridier *et al.*[9]	FP/UV	760	298	3.4 ± 1.0
Larichev *et al.*[8]	DF/MS	1	233–344	$(0.48 \pm 0.03)\exp[(580 \pm 100)/T]$
Elrod *et al.*[10]	DF/MS	100	210–298	$(0.25 \pm 0.08)\exp[(520 \pm 80)/T]$
this work	DF/MS	1	233–348	$(0.31 \pm 0.03)\exp[(540 \pm 210/T)]$

[a] MP/UV = modulated photolysis/UV absorption; FP/UV = flash photolysis/UV absorption; DF/MS = discharge-flow/mass spectrometry

source of Br in the flow tube. Simulations show that most of the Br reacts with O_3, which regenerates BrO and suppresses the concentration of Br to the point where removal of HO_2 by Br can neglected.

Comparison of results with previous studies

The results of previous kinetics studies of the $HO_2 + BrO$ reaction are summarized in Table 4 and in Fig. 9. The measured values of k_{298} fall into three groups: the early measurement of Cox and Sheppard at 5×10^{-12} cm^3 molecule^{-1} s^{-1},[6] the considerably higher values around 3.3×10^{-11} from Poulet *et al.*,[7] Larichev *et al.*[8] and Bridier *et al.*,[9] and the intermediate values in the range $(1.4–2.0) \times 10^{-11}$ cm^3 molecule^{-1} s^{-1} from Elrod *et al.*[10] and this work. The significant difference between the results from this work and the two studies of the Orleans group is puzzling because both groups used discharge-flow/mass spectrometry systems at low pressure with similar radical sources. There are, however, some differences in methodology which may account for the disagreement. Both studies used the $Cl + CH_3OH$ reaction to produce HO_2. This source is strongly affected by wall reactions below *ca.* 250 K as observed in both studies. Larichev *et al.* dealt with this problem by producing HO_2 in a side-arm at room temperature in the flow tube. This approach eliminates problems associated with the reduced efficiency of the source at low temperature, but since the excess reagent (HO_2) is not injected from the movable inlet, the first-order wall loss of HO_2 contributes to the measured first-order rate constant. Complications associated with the $Cl + CH_3OH$ source at low temperatures were circumvented in the present study by always keeping the sliding injector source at room temperature using the integral heating coil. This approach maintains the advantage of introducing the excess reagent through the sliding injector.

The values of k_{298} obtained in the three temperature dependence studies range over a factor of about 2.4 but the measured values of E/R are remarkably similar as seen in Table 4. All three studies report a moderately negative temperature dependence with the values ranging from -520 to -580 K^{-1}. In the study of Larichev *et al.*, the measurement of k_3 at 233 K was not considered in the determination of E/R because it fell considerably off the Arrhenius line described by their 243–344 K data. In the present work the Arrhenius plot was linear over the 233–348 K temperature range, and in the study of Elrod *et al.* the plot was linear over the range 210–298 K.

Reaction mechanism

The mechanism for the formation of HOX from $HO_2 + XO$, where X = Cl or Br, has not been established with certainty but *ab initio* calculations are available which provide estimates of the stabilities of the possible reaction intermediates. In the system involving Cl, Francisco and Sander calculated enthalpies of formation for several $HClO_3$ isomers using both isodesmic reactions at the QCISD(T)/6-311G(2df,2p) level and G1/G2 theory.[25] Values of $\Delta_f H^\circ_0$ (in kcal mol^{-1}) were determined to be $HOClO_2$ (4.2), HOOOCl (9.1), HOOClO (25) and $HClO_3$ (46.1). For HOOClO and HOOOCl these results are significantly different from the values obtained from the bond additivity calculations of Stimpfle *et al.*[26] The most stable isomer, $HOClO_2$ is unlikely to form from $HO_2 + ClO$ because of the extensive rearrangement required. The next most stable intermediate, HOOOCl, is the likely intermediate in the reaction pathway leading to HCl through formation of a five-membered transition state followed by HCl elimination; however, the small branching ratio measured for this pathway implies the existence of a significant exit channel barrier.[27–29] The likely intermediate in the formation of HOCl is HOOClO as suggested by Stimpfle *et al.*[26] because the observed negative temperature dependence is more consistent with a mechanism involving a strongly bound intermediate (HOOClO) than the weakly bound intermediate involved in hydrogen abstraction (ClOHOO).

The thermochemistry of the $HO_2 + BrO$ system is qualitatively similar to its chlorine counterpart. The $BrO + HO_2$ reaction has several exothermic reaction pathways:

$$BrO + HO_2 \rightarrow HOBr + O_2 \qquad \Delta_f H^\circ_{298} = -46.5 \pm 4 \text{ kcal mol}^{-1} \quad (3a)$$

$$\rightarrow HBr + O_3 \qquad \Delta_f H^\circ_{298} = -7.1 \pm 2 \text{ kcal mol}^{-1} \quad (3b)$$

$$\xrightarrow{[M]} HO_2 \cdot BrO \quad (3c)$$

where $HO_2 \cdot BrO$ denotes a collisionally stabilized adduct. Several previous studies including the present work found that reaction (3a) was an important, if not the predominant, reaction channel but were not able to establish that the branching ratio for reaction (3a) was unity.[8,10] On the other hand, there is positive evidence that the branching ratio for reaction (3b) is quite small. Larichev *et al.* were unable to detect O_3 in their study of reaction (3) and set an upper limit of 0.015 for k_{3b}/k_3 over the temperature range 233–298 K. Mellouki *et al.* inferred an upper limit of *ca.* 1×10^{-4} for k_{3b}/k_3 at 300 K based on studies of the reverse reaction,

$$HBr + O_3 \rightarrow HO_2 + BrO \quad (-3b)$$

using laser magnetic resonance detection of HO_2.[30] There have been no indications from any previous study that reaction (3) results in the formation of a stable adduct as indicated in reaction (3c). *Ab initio* calculations by Guha and Francisco[31] at the B3LYP/6-311++G(3df,3pd) level show that the enthalpies of formation of $HBrO_3$ isomers increase in the order $HOBrO_2 < HOOOBr < HOOBrO < HBrOOO$. This is the same ordering as the analogous system involving chlorine. While absolute energies for $HBrO_3$ isomers are not yet available, it is clear from the observed negative temperature dependence of the HOBr channel that potential-energy surfaces are qualitatively similar to the chlorine system. The 298 K rate constants for the $HO_2 + XO$ reactions increase significantly as X is substituted in the order Cl < Br < I. Bogan *et al.* have attributed this to the increasing tendency of the larger XO species to access the available triplet surfaces through spin–orbit coupling.[24] Other factors that may contribute to the observed rate constant enhancement are stronger long-range interactions between HO_2 and XO, and progressive loosening of the HOOXO transition state.

Atmospheric implications

The combined results of this study and the work of Elrod *et al.* strengthen the case for a smaller rate coefficient for reaction (3) than the value that appears in the 1994 NASA Data Evaluation. This will have the effect of slightly lowering the overall catalytic destruction rate of ozone by bromine, and consequently the ozone depletion potential of CH_3Br. The reduction in k_3 will have the effect of repartitioning bromine from HOBr into BrO, which will increase the rate of the $BrO + ClO$ cycle, partially offsetting the effect on the $HO_2 + BrO$ cycle.

Summary

We have studied the kinetics of the reaction of BrO with HO_2 over the temperature range 233–348 K using the technique of discharge-flow/mass spectrometry. Variations in experimental conditions such as flow velocity, reactor total pressure, and the excess reactant (HO_2 or BrO) had no effect on the mea-

sured rate coefficients within the 2σ error limits. At 298 K, the rate coefficient was determined to be $(1.73 \pm 0.61) \times 10^{-11}$ cm^3 $molecule^{-1}$ s^{-1} with HO_2 in excess and $(2.05 \pm 0.64) \times 10^{-11}$ cm^3 $molecue^{-1}$ s^{-1} with BrO in excess, respectively. The combined data from the excess BrO and excess HO_2 experiments were fit to an Arrhenius expression which gave $k_3 = (3.13 \pm 0.33) \times 10^{-12}$ $\exp(536 \pm 206/T)$. These results obtained here, along with the measurements of Elrod *et al.* contrast with three recent studies giving 298 K rate constants that are about a factor of two larger. The reasons for the discrepancy are not well understood.

This research was performed by the Jet Propulsion Laboratory, California Institute Technology, under contract with National Aeronautics and Space Administration. We are grateful to J. S. Francisco and S. Guha for providing details of their *ab initio* calculations on $HBrO_3$, and to David Natzic and Juergen Linke for their expert technical assistance in this work.

References

1 *WMO*, *Scientific Assessment of Ozone Depletion*: *1994*, National Aeronautics and Space Administration, 1994.
2 S. C. Wofsy, M. D. McElroy and Y. L. Yung, *Geophys. Res. Lett.* 1975, **2**, 215.
3 Y. L. Yung, J. P. Pinto, R. T. Watson and S. P. Sander, *J. Atmos. Sci.*, 1980, **37**, 339.
4 W. B. More, D. M. Golden, R. F. Hampson, C. J. Howard, M. J. Kurylo, M. J. Molina, A. R. Ravishankara and S. P. Sander, in *Chemical Kinetics and Photochemical Data for Use in Stratospheric Modeling*, Pasadena, CA, 1994.
5 R. Atkinson, D. L. Baulch, R. A. Cox, R. F. Hampson, J. A. Kerr and J. Troe, *J. Phys. Chem. Ref. Data*, 1992, **21**, 1125.
6 R. A. Cox and D. W Sheppard, *J. Chem. Soc., Faraday Trans. 2*, 1982, **78**, 1383.
7 G. Poulet, M. Pirre, F. Maguin, R. Ramaroson and G. Le Bras, *Geophys. Res. Lett.*, 1992, **19**, 2305.
8 M. Larichev, F. Maguin, G. Le Bras and G. Poulet, *J. Phys. Chem.*, 1995, **99**, 15911.
9 I. Bridier, B. Veyret and R. Lesclaux, *Chem. Phys. Lett.*, 1993, **201**, 563.
10 M. J. Elrod, R. F. Meads, J. B. Lipson, J. V. Seeley and M. J. Molina, *J. Phys. Chem.*, 1996, **100**, 5808.
11 G. W. Ray, L. F. Keyser and R. T. Watson, *J. Phys. Chem.*, 1980, **84**, 1674.
12 R. R. Friedl and S. P. Sander, *J. Phys. Chem.*, 1989, **93**, 4756.
13 M. A. A. Clyne, P. B. Monkhouse and L. W. Townsend, *Int. J. Chem. Kinet.*, 1976, **8**, 425.
14 C-D. Walther and H. G. Wagner, *Ber. Bunsen-Ges. Phys. Chem.*, 1983, **87**, 403.
15 S. P. Sander, *J. Phys. Chem.*, 1984, **88**, 6018.
16 C. J. Howard, *J. Chem. Phys.* 1976, **65**, 4771.
17 J. P. D. Abbatt and J. G. Anderson, *J. Phys. Chem.*, 1991, **95**, 2382.
18 T. R. Marrero and E. A. Mason, *J. Phys. Chem. Ref. Data*, 1972, **1**, 3.
19 N. I. Butkovskaya, I. I. Morozov, V. J. Talrose and E. S. Vasiliev, *Chem. Phys.*, 1983, **79**, 21.
20 O. V. Rattigan, R. A. Cox and R. L. Jones, *J. Chem. Soc., Faraday Trans.*, 1995, **91**, 4189.
21 C. E. Miller, S. L. Nickolaisen and S. P. Sander, *J. Chem. Phys.*, in press.
22 O. V. Rattigan, R. L. Jones and R. A. Cox, *Chem. Phys. Lett.*, 1994 **230**, 121.
23 H. S. P. Mueller, C. E. Miller and E. A. Cohen, *Angew. Chem.*, 1996, **35**, 2005.
24 D. J. Bogan, R. P. Thorn, F. L. Nesbitt and L. J. Stief, *J. Phys. Chem.*, 1996, **100**, 14383.
25 J. S. Francisco and S. P. Sander, *J. Phys. Chem.* 1996, **100**, 573.
26 R. Stimpfle, R. Perry and C. J. Howard, *J. Chem. Phys.*, 1979, **71**, 5183.
27 M. T. Leu, *Geophys. Res. Lett.*, 1980 **72**, 2364.
28 T. J. Leck, J. E. Cook and J. W. Birks, *J. Chem. Phys.*, 1980, **72**, 2364.
29 M. Finkbeiner, J. N. Crowley, O. Horie, R. Muller, G. K. Moortgat and P. J. Crutzen, *J. Geophys. Res.*, 1994, **99**, 16264.
30 A. Mellouki, R. K. Talukdar and C. J. Howard, *J. Geophys. Res.*, 1994, **99**, 22949.
31 S. Guha and J. S. Francisco, 1997, unpublished work.

Paper 7/01583F; *Received 6th March*, 1997